Orbital-Fluctuation-Mediated Superconductivity in Iron Pnictides: Analysis of the Five-Orbital Hubbard-Holstein Model

Hiroshi Kontani[1] and Seiichiro Onari[2]

[1]Department of Physics, Nagoya University and JST, TRIP, Furo-cho, Nagoya 464-8602, Japan
[2]Department of Applied Physics, Nagoya University and JST, TRIP, Furo-cho, Nagoya 464-8602, Japan

(Received 11 December 2009; published 15 April 2010)

In iron pnictides, we find that the moderate electron-phonon interaction due to the Fe-ion oscillation can induce the critical d-orbital fluctuations, without being prohibited by the Coulomb interaction. These fluctuations give rise to the strong pairing interaction for the s-wave superconducting (SC) state without sign reversal (s_{++}-wave state), which is consistent with experimentally observed robustness of superconductivity against impurities. When the magnetic fluctuations due to Coulomb interaction are also strong, the SC state shows a smooth crossover from the s-wave state with sign reversal ($s_{\pm}$-wave state) to the s_{++}-wave state as impurity concentration increases.

DOI: 10.1103/PhysRevLett.104.157001 PACS numbers: 74.70.Xa, 74.20.Rp

The mechanism of high-T_c superconductivity in iron pnictides has been an important open problem. By considering the Coulomb interaction at Fe ions, an antiferromagnetic (AFM) fluctuation mediated fully-gapped sign-reversing s-wave state ($s_{\pm}$-wave state) is expected theoretically [1,2]. Regardless of the beauty of the mechanism, there are several serious discrepancies for the $s_{\pm}$-wave state. For example, although the $s_{\pm}$-wave state is expected to be very fragile against impurities due to the interband scattering [3], the superconducting (SC) state is remarkably robust against impurities [4] and α-particle irradiation [5]. Moreover, clear ''resonancelike'' peak structure observed by neutron scattering measurements [6] is reproduced by considering the strong correlation effect via quasiparticle damping, without the necessity of sign reversal in the SC gap [7]. These facts indicate that a conventional s-wave state without sign reversal (s_{++}-wave state) is also a possible candidate for iron pnictides.

Then, a natural question is whether the electron-phonon (e-ph) interaction is important or not. Although first principle study predicts a small e-ph coupling constant $\lambda \sim 0.21$ [8], several experiments indicate the significance of the e-ph interaction. For example, the structural transition temperature T_S is higher than the Néel temperature in underdoped compounds, although the structural distortion is small. Also, prominent softening of the shear modulus is observed towards T_S or T_c in Ba122 [9]. Raman spectroscopy [10] also indicates larger e-ph interaction.

Interestingly, there are several ''high-T_c'' compounds with nodal SC gap structure, like $BaFe_2(As_{1-x}P_x)_2$ [11] and some 122 systems [12]. Although the nodal $s_{\pm}$-wave state can appear in the spin-fluctuation scenario due to the competition between the dominant $\boldsymbol{Q} = (\pi, 0)$ and subdominant fluctuations [1,13], the T_c is predicted to be very low. Thus, it is a crucial challenge to explain the rich variety of the gap structure in high-T_c compounds.

In this Letter, we introduce the five-orbital Hubbard-Holstein (HH) model for iron pnictides, considering the e-ph interaction by Fe-ion vibrations. We reveal that a relatively small e-ph interaction ($\lambda \lesssim 0.3$) induces the large orbital fluctuations, which can realize the high-T_c s_{++}-wave SC state. Moreover, the orbital fluctuations are *accelerated* by Coulomb interaction. In the presence of impurities, the s_{++}-wave state dominates the $s_{\pm}$-wave state for a wide range of parameters.

First, we derive the e-ph iteration term, considering only Einstein-type Fe-ion oscillations for simplicity. Here, we describe the d orbitals in the XYZ coordinate [1], which is rotated by $\pi/4$ from the xyz coordinate given by the Fe-site square lattice: We write the Z^2, XZ, YZ, $X^2 - Y^2$, and XY orbitals as 1, 2, 3, 4, and 5, respectively [1]. We calculate the e-ph matrix elements due to the Coulomb potential, by following Ref. [14]. The potential for a d electron at $\boldsymbol{r}$ (with the origin at the center of the Fe ion) due to the surrounding As^{3-}-ion tetrahedron is $U^{\pm}(\boldsymbol{r};\boldsymbol{u}) = 3e^2 \sum_{s=1}^{4} |\boldsymbol{r} + \mathbf{u} - \boldsymbol{R}_s^{\pm}|^{-1}$, where $\boldsymbol{u}$ is the displacement vector of the Fe ion, and $\boldsymbol{R}_s^{\pm}$ is the location of the surrounding As ions; $\sqrt{3}\boldsymbol{R}_s^{+}/R_{\mathrm{Fe-As}} = (\pm\sqrt{2}, 0, 1)$ and $(0, \pm\sqrt{2}, -1)$ for $Fe^{(1)}$, and $\sqrt{3}\boldsymbol{R}_s^{-}/R_{\mathrm{Fe-As}} = (\pm\sqrt{2}, 0, -1)$ and $(0, \pm\sqrt{2}, 1)$ for $Fe^{(2)}$ in the unit cell with two Fe-sites. Note that $u_{X,Y}$ and u_Z belong to E_g and B_{1g} phonons [10]. The $\boldsymbol{u}$ linear term of $U^{\pm}$, which gives the e-ph interaction, is obtained as $V^{\pm}(\boldsymbol{r};\boldsymbol{u}) = \pm A[2XZu_X - 2YZu_Y + (X^2 - Y^2)u_Z] + O(\boldsymbol{r}^4)$, where $A = 30e^2/\sqrt{3}R_{\mathrm{Fe-As}}^4$. Then, its nonzero matrix elements are given as

$$\begin{aligned} \langle 2|V|4\rangle &= \pm 2a^2 A u_X/7, \quad & \langle 3|V|4\rangle &= \pm 2a^2 A u_Y/7, \\ \langle 2|V|2\rangle &= \pm 2a^2 A u_Z/7, \quad & \langle 3|V|3\rangle &= \mp 2a^2 A u_Z/7, \end{aligned} \tag{1}$$

where a is the radius of the d orbital. Here, we consider $\langle i|V|j\rangle$ only for orbitals $i, j = 2$–4 that compose the Fermi surfaces (FSs) in Fig. 1(a) [1]. The obtained e-ph interaction does not couple to the charge density since $\langle i|V|j\rangle$ is traceless. Thus, the Thomas-Fermi screening for the coefficient A is absent. The local phonon Green function is $D(\omega_l) = 2\bar{u}_0^2\omega_D/(\omega_l^2 + \omega_D^2)$, which is given by the

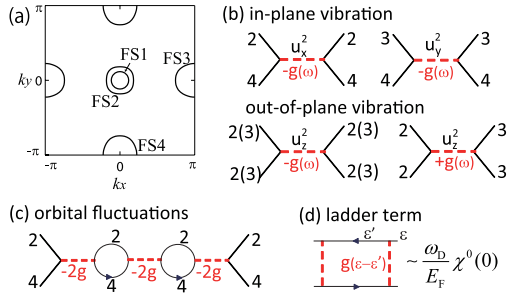

FIG. 1 (color online). (a) FSs in the unfolded Brillouin zone. (b) Phonon-mediated electron-electron interaction. (c) A bubble-type diagram that induces the critical orbital fluctuations between (2,4) orbitals. (d) A ladder-type diagram that is ignorable when $\omega_D \ll E_F$.

Fourier transformation of $\langle T_\tau u_\mu(\tau) u_\mu(0)\rangle$ ($\mu = X, Y, Z$). $\bar{u}_0 = \sqrt{\hbar/2M_{\mathrm{Fe}}\omega_D}$ is the position uncertainty of Fe ions, ω_D is the phonon frequency, and $\omega_l = 2\pi l T$ is the boson Matsubara frequency. Then, for both $\mathrm{Fe}^{(1)}$ and $\mathrm{Fe}^{(2)}$, the phonon-mediated interaction is given by

$$V_{24,42} = V_{34,43} = -(2Aa^2/7)^2 D(\omega_l) \equiv -g(\omega_l),$$
$$V_{22,22} = V_{33,33} = -V_{22,33} = -g(\omega_l), \tag{2}$$

as shown in Fig. 1(b). Note that $V_{ll',mm'}$ is symmetric with respect to $l \leftrightarrow l'$, $m \leftrightarrow m'$, and $(ll') \leftrightarrow (mm')$. We obtain $g(0) \approx 0.4$ eV if we put $R_{\mathrm{Fe-As}} \approx 2.4$ Å, $a \approx 0.77$ Å (Shannon crystal radius of Fe^{2+}), and $\omega_D \approx 0.018$ eV. We have neglected the e-ph coupling due to d-p hybridization [14] considering the modest d-p hybridization in iron pnictides [15]. Thus, we obtain the multiorbital HH model for iron pnictides by combining Eq. (2) with the on-site Coulomb interaction; the intra- (inter-) orbital Coulomb U (U'), Hund coupling J, and pair hopping J'.

Now, we study the rich electronic properties realized in the multiorbital HH model [16]. The irreducible susceptibility in the five-orbital model is given by $\chi^0_{ll',mm'}(q) = -(T/N)\sum_k G^0_{lm}(k+q) G^0_{m'l'}(k)$, where $\hat{G}^0(k) = [i\epsilon_n + \mu - \hat{H}^0_{\boldsymbol{k}}]^{-1}$ is the d-electron Green function in the orbital basis: $q = (\boldsymbol{q}, \omega_l)$, $k = (\boldsymbol{k}, \epsilon_n)$, and $\epsilon_n = (2n+1)\pi T$ is the fermion Matsubara frequency. μ is the chemical potential, and $\hat{H}^0_{\boldsymbol{k}}$ is the kinetic term given in Ref. [1]. Then, the susceptibilities for spin and charge sectors in the random phase approximation (RPA) are given as [17]

$$\hat{\chi}^{s(c)}(q) = \hat{\chi}^0(q)[1 - \hat{\Gamma}^{s(c)}\hat{\chi}^0(q)]^{-1}. \tag{3}$$

For the spin channel, $\Gamma^s_{l_1 l_2, l_3 l_4} = U, U', J$, and J' for $l_1 = l_2 = l_3 = l_4$, $l_1 = l_3 \neq l_2 = l_4$, $l_1 = l_2 \neq l_3 = l_4$, and $l_1 = l_4 \neq l_2 = l_3$, respectively [1]. For the charge channel, $\hat{\Gamma}^c = -\hat{C} - 2\hat{V}(\omega_l)$, where $\hat{V}(\omega_l)$ is given in Eq. (2), and $C_{l_1 l_2, l_3 l_4} = U, -U' + 2J, 2U' - J$, and J' for $l_1 = l_2 = l_3 = l_4$, $l_1 = l_3 \neq l_2 = l_4$, $l_1 = l_2 \neq l_3 = l_4$, and $l_1 = l_4 \neq l_2 = l_3$, respectively [1]. Figure 1(c) shows one of the bubble diagrams for the (2,4)-channel due to the "negative exchange coupling $V_{24,42}$" that leads to a critical enhancement of $\hat{\chi}^c(q)$ [18]. We neglect the ladder diagrams given by $\hat{V}(\omega_l)$ in Fig. 1(d) since $\omega_D \ll W_{\mathrm{band}}$ [8,10]. We put $\omega_D = 0.02$ eV, $U'/U = 0.69$, $J/U = 0.16$, and $J = J'$, and fix the electron number $n = 6.1$ (10% electron doping); the density of states per spin is $N(0) = 0.66\ \mathrm{eV}^{-1}$. Numerical results are not sensitive to these parameters. We use 128^2 $\boldsymbol{k}$ meshes, and 512 Matsubara frequencies. Hereafter, the unit of energy is eV.

Figure 2(a) shows the obtained U-$g(0)$ phase diagram. $\alpha_{s(c)}$ is the spin (charge) Stoner factor, given by the maximum eigenvalue of $\hat{\Gamma}^{s(c)}\hat{\chi}^0(\boldsymbol{q}, 0)$. Then, the enhancement factor for $\chi^{s(c)}$ is $(1 - \alpha_{s(c)})^{-1}$, and $\alpha_{s(c)} = 1$ gives the spin (orbital) order boundary. Because of the nesting of the FSs, the AFM fluctuation with $\boldsymbol{Q} \approx (\pi, 0)$ develops as U increases, and $s_\pm$-wave state is realized for $\alpha_s \lesssim 1$ [1]. In contrast, we find that the orbital fluctuations develop as $g(0)$ increases. For $U = 1$, the critical value $g_{\mathrm{cr}}(0)$ for $\alpha_c = 1$ is 0.4, and the critical e-ph coupling constant is $\lambda_{\mathrm{cr}} \equiv g_{\mathrm{cr}}(0)N(0) = 0.26$ [19]. Since the obtained λ_{cr} is close to λ given by the first principle study [8], strong orbital fluctuations are expected to occur in iron pnictides. At fixed U, λ_{cr} decreases as J/U approaces zero.

Figures 2(b) and 2(c) show the obtained $\chi^c_{ll',mm'}(\boldsymbol{q}, 0)$ for $(ll', mm') = (24, 42)$ and $(22, 22)$, respectively, for $U = 1.14$ and $\alpha_c = 0.97$ ($g(0) = 0.40$): Both of them are the most divergent channels for electron-doped cases. The enhancement of (24, 42)-channel is induced by the multiple scattering by $V_{24,42}$. The largest broad peak around $\boldsymbol{q} = (0, 0)$ originates from the forward scattering in the electron-pocket (FS3 or 4) composed of 2–4 orbitals. (FS1,2 are composed of only 2 and 3 orbitals.) These ferro-orbital fluctuations would induce the softening of shear modulus [9], and also reinforce the ferro-orbital-ordered state below T_S [20] that had been explained by

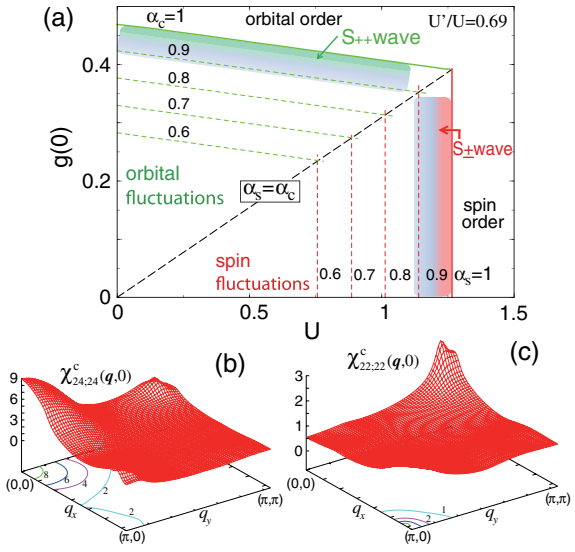

FIG. 2 (color online). (a) Obtained U-$g(0)$ phase diagram. (b) Obtained $\chi^c_{24,42}(\boldsymbol{q}, 0)$ and $\chi^c_{22,22}(\boldsymbol{q}, 0)$ for $\alpha_c = 0.97$.

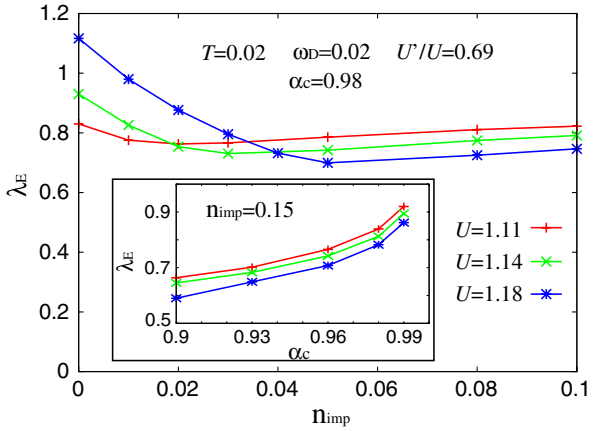

FIG. 3 (color online). n_{imp} dependence of λ_E at $\alpha_c = 0.98$. If we put $g(0) = 0$ ($s_\pm$ state), λ_E at $n_{\mathrm{imp}} = 0$ decreases by $0.1 \sim 0.15$, since the ferro-orbital fluctuations enhance both the s_{++} and $s_\pm$ wave states. Inset: α_c dependence of λ_E.

different theoretical approaches [21]: The divergence of $\chi^c_{24,42}$ ($\chi^c_{34,43}$) pushes the 2,4 (3,4) orbitals away from the Fermi level, and the Fermi surfaces in the ordered state will be formed only by 3 (2) orbital, consistently with ref. [20]. The lower peak around $\boldsymbol{Q} = (\pi, 0)$ comes from the nesting between hole- and electron-pockets. Also, the enhancement of (22, 22)-channel for $\boldsymbol{Q} = (\pi, 0)$ is induced by the nesting via multiple scattering by $V_{22,22}$ and $V_{22,33}$. In contrast, the charge susceptibility $\sum_{l,m}\chi^c_{ll,mm}(\boldsymbol{q}, 0)$ is finite even if $\alpha_c \to 1$ since $\chi^c_{22,33} \approx -\chi^c_{22,22}$.

Now, we will show that large orbital fluctuations, which are not considered in the first principle study of T_c [8], can induce the s_{++}-wave state when $g(0) > 0$. We analyze the following linearized Eliashberg equation using the RPA [1], by taking both the spin and orbital fluctuations into account on the same footing:

$$\lambda_E \Delta_{ll'}(k) = \frac{T}{N}\sum_{k',m_i} W_{lm_1,m_4l'}(k-k') G_{m_1m_2}(k') \Delta_{m_2m_3}(k') \times G_{m_4m_3}(-k'), \quad (4)$$

where $\hat{W}(q) = -\frac{3}{2}\hat{\Gamma}^s \hat{\chi}^s(q)\hat{\Gamma}^s + \frac{1}{2}\hat{\Gamma}^c \hat{\chi}^c(q)\hat{\Gamma}^c - \frac{1}{2}(\hat{\Gamma}^s - \hat{\Gamma}^c)$ for singlet states. The eigenvalue λ_E increases as $T \to 0$, and it reaches unity at $T = T_c$. In addition, we take the impurity effect into consideration since many iron pnictides show relatively large residual resistivity. Here, we assume the Fe-site substitution, where the impurity potential I is diagonal in the d-orbital basis [3]. Then, the T matrix in the normal state is given by $\hat{T}(\epsilon_n) = [I^{-1} - N^{-1}\sum_{\boldsymbol{k}} \hat{G}(\boldsymbol{k}, \epsilon_n)]^{-1}$ in the orbital basis [3]. Then, the normal self-energy is $\hat{\Sigma}^n(\epsilon_n) = n_{\mathrm{imp}}\hat{T}(\epsilon_n)$, where n_{imp} is the impurity concentration. Also, the linearized anomalous self-energy is given by

$$\Sigma^a_{ll'}(\epsilon_n) = \frac{n_{\mathrm{imp}}}{N}\sum_{\boldsymbol{k},m_i} T_{lm_1}(\epsilon_n) G_{m_1m_2}(\boldsymbol{k}, \epsilon_n) \Delta_{m_2m_3}(\boldsymbol{k}, \epsilon_n) \times G_{m_4m_3}(-\boldsymbol{k}, -\epsilon_n) T_{l'm_4}(-\epsilon_n). \quad (5)$$

Then, the Eliashberg equation for $n_{\mathrm{imp}} \neq 0$ is given by using the full Green function $\hat{G}(k) = [i\epsilon_n + \mu - \hat{H}^0_{\boldsymbol{k}} - \hat{\Sigma}^n(\epsilon_n)]^{-1}$ in Eqs. (4) and (5), and adding $\Sigma^a_{ll'}(\epsilon_n)$ to the right hand side of Eq. (4). Hereafter, we solve the equation at relatively high temperature $T = 0.02$ since the number of $\boldsymbol{k}$ meshes (128^2) is not enough for $T < 0.02$.

Figure 3 shows the n_{imp} dependence of λ_E at $\alpha_c = 0.98$, for $U = 1.11$, 1.14 and 1.18. Considering large $\lambda_E \gtrsim 0.8$ at $T = 0.02$, relatively high-T_c ($\lesssim 0.02$) is expected. For the smallest U ($U = 1.11$; $\alpha_s = 0.85$), we find that nearly isotropic s_{++}-wave state is realized; the obtained λ_E is almost independent of n_{imp}, indicating the absence of the impurity effect on the s_{++}-wave state, as discussed in Refs. [3,22]. For the largest U ($U = 1.18$; $\alpha_s = 0.91$), the $s_\pm$-wave state is realized at $n_{\mathrm{imp}} = 0$; λ_E decreases slowly as n_{imp} increases from zero, whereas it saturates for $n_{\mathrm{imp}} \geq 0.05$, indicating the smooth crossover from $s_\pm$- to s_{++}-wave states due to the interband impurity scattering. For $U = 1.14$ ($\alpha_s = 0.88$), the SC gap at $n_{\mathrm{imp}} = 0$ is a hybrid of s_{++} and $s_\pm$; only Δ_{FS2} is different in sign.

The inset of Fig. 3 shows λ_E for the s_{++}-wave state in the presence of impurities: Since $\lambda_E(\alpha_c = 0.98) - \lambda_E(\alpha_c = 0.9)$ is only $\sim$0.15 for each value of U, we expect that relatively large T_c for s_{++}-wave state is realized even if orbital fluctuations are moderate. We stress that the obtained λ_E is almost constant for $\omega_D = 0.02$–0.1, suggesting the absence of isotope effect in the s_{++}-wave state due to the strong retardation effect [14]. By the same reason, λ_E for the s_{++}-wave state is seldom changed if we put $U = 3$ in the Hartree-Fock term $\frac{1}{2}(\hat{\Gamma}^s - \hat{\Gamma}^c)$ in $W(q)$, indicating that the Morel-Anderson pseudopotential almost saturates.

Here, we discuss the case $U = 1.18$ in detail: Fig. 4 shows the SC gap on the FSs in the band representation for (a) $n_{\mathrm{imp}} = 0$, (b) 0.03, and (c) 0.08. They satisfy the condition $N^{-1}\sum_{\boldsymbol{k},lm}|\Delta_{lm}(\boldsymbol{k})|^2 = 1$. The horizontal axis is the azimuth angle for the $\boldsymbol{k}$ point with the origin at Γ (M) point for FS1,2 (FS4); $\theta = 0$ corresponds to the k_x direction. In case (a), the $s_\pm$ state with strong imbalance, $|\Delta_{\mathrm{FS1}}|, |\Delta_{\mathrm{FS2}}| \ll \Delta_{\mathrm{FS4}}$, is realized, and Δ_{FS4} takes the largest value at $\theta = \pi/2$, where the FS is mainly composed of orbital 4. In case (c), the impurity-induced isotropic s_{++} state [23] with $\Delta_{\mathrm{FS1}} \sim \Delta_{\mathrm{FS2}} \sim \Delta_{\mathrm{FS34}}$ is realized, consistently with many ARPES measurements [24]. In case (b), $\Delta_{\boldsymbol{k}}$ on FS1 is almost gapless. However, considering the k_z dependence of the FSs, a (horizontal-type) nodal structure is expected to appear on FS1,2. In real compounds with $T_c \sim 50$ K, the $s_\pm \to s_{++}$ crossover should be induced by small residual resistivity $\rho_{\mathrm{imp}} \sim 20\ \mu\Omega$cm ($n_{\mathrm{imp}} \sim 0.01$ for $I = 1$), as estimated in Ref. [3].

We comment that at $n_{\mathrm{imp}} = 0$, $s_\pm$-wave state is realized in the RPA even if $\alpha_s \lesssim \alpha_c$, due to factor 3 in front of $\frac{1}{2}\hat{\Gamma}^s \hat{\chi}^s(q)\hat{\Gamma}^s$ in $W(q)$. For the same reason, however, reduction in α_s (or increment of U_{cr} for $\alpha_s = 1$) due to the "self-energy correction by U" is larger, which will be unfavor-

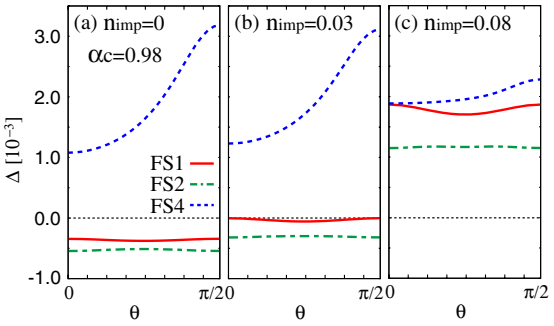

FIG. 4 (color online). SC gap functions for $U = 1.18$ as functions of θ at (a) $n_{\rm imp} = 0$, (b) 0.03, and (c) 0.08, respectively.

able for the $s_{\pm}$-wave state. Therefore, self-consistent calculation for the self-energy is required to discuss the value of $\alpha_{c,s}$ and the true pairing state.

Here, we discuss where in the α_s-α_c phase diagram in Fig. 2(a) real compounds are located. Considering the weak T dependence of $1/T_1T$ in electron-doped SC compounds [25], we expect that they belong to the area $\alpha_c \gg \alpha_s$. Then, the s_{++}-wave SC state will be realized without (or very low density) impurities, like the case of $U = 1.11$ or 1.14 in Fig. 3. On the other hand, impurity-induced $s_{\pm} \rightarrow s_{++}$ crossover may be realized in $BaFe_2(As_{1-x}P_x)_2$ (undoped) or $(Ba_{1-x}K_x)Fe_2As_2$ (hole-doped) SC compounds, where AFM fluctuations are rather strong.

Finally, we discuss the non-Fermi-liquid-like transport phenomena in iron pnictides. For example, the resistivity is nearly linear in T, and the Hall coefficient R_H increases at lower temperatures [4,26]. Although the forward scattering induced by ferro-orbital fluctuations might be irrelevant, antiferro-orbital and AFM fluctuations with $\boldsymbol{Q} = (\pi, 0)$ are expected to cause the anomalous transport, due to the current vertex correction [27].

In summary, we have proposed a mechanism of the s_{++}-wave SC state induced by orbital fluctuations, due to the phonon-mediated electron-electron interaction. Three orbitals (XZ, YZ, and $X^2 - Y^2$) are necessary to lead the ferro-orbital fluctuations. The SC gap structure drastically changes depending on parameters α_s, α_c, and $n_{\rm imp}$, consistent with the observed rich variety of the gap structure that is a salient feature of iron pnictides. The orbital-fluctuation-mediated s_{++}-wave state is also obtained for hole-doped cases, although the antiferro-orbital fluctuations become stronger than the ferro-orbital ones.

The s-wave superconductivity induced by orbital fluctuations had been discussed in Ref. [17] for $U' > U$; this condition can be realized by including the A_{1g} phonon [28]. In the present model, however, the A_{1g} phonon is negligible since $g_{\rm cr}(0)$ given by the A_{1g} phonon is much greater than $g_{\rm cr}(0) \sim 0.4$ in Fig. 2(a): The ferro-obtital fluctuations in Fig. 2(b) originate from the *negative* exchange interaction caused by the E_g phonon, as shown in Fig. 1(c).

We thank D. S. Hirashima, M. Sato, Y. Matsuda, Y. Ōno, and Y. Yanagi for valuable discussions. This study has been supported by Grants-in-Aid for Scientific Research from MEXT of Japan, and by JST, TRIP.

Note added in proof.—After the acceptance of this work, we found that $g_{\rm cr}(0) \sim 0.4$ in Fig. 2(a) reduced to half if all the e-ph matrix elements including the 1,5 orbitals are taken into account. Results similar to Fig. 3 are obtained by using $g(0) \sim 0.2$, whereas (vertical-type) nodes appear on FS3,4 during the $s_{++} \rightarrow s_{\pm}$ crossover for $U = 1.18$.

[1] K. Kuroki *et al.*, Phys. Rev. Lett. **101**, 087004 (2008).
[2] I. I. Mazin *et al.*, Phys. Rev. Lett. **101**, 057003 (2008).
[3] S. Onari and H. Kontani, Phys. Rev. Lett. **103**, 177001 (2009).
[4] A. Kawabata *et al.*, J. Phys. Soc. Jpn. **77**, Suppl. C, 103704 (2008); M. Sato *et al.*, J. Phys. Soc. Jpn. **79**, 014710 (2009); S. C. Lee *et al.*, J. Phys. Soc. Jpn. **79**, 023702 (2010).
[5] C. Tarantini *et al.*, arXiv:0910.5198.
[6] A. D. Christianson *et al.*, Nature (London) **456**, 930 (2008).
[7] S. Onari, H. Kontani, and M. Sato, Phys. Rev. B **81**, 060504(R) (2010).
[8] L. Boeri, O. V. Dolgov, and A. A. Golubov, Phys. Rev. Lett. **101**, 026403 (2008).
[9] R. M. Fernandes *et al.*, arXiv:0911.3084.
[10] M. Rahlenbeck *et al.*, Phys. Rev. B **80**, 064509 (2009).
[11] K. Hashimoto *et al.*, arXiv:0907.4399.
[12] C. Martin *et al.*, Phys. Rev. B **81**, 060505(R) (2010).
[13] T. A. Maier *et al.*, Phys. Rev. B **79**, 224510 (2009).
[14] K. Yada and H. Kontani, Phys. Rev. B **77**, 184521 (2008).
[15] D. J. Singh, Physica (Amsterdam) **469C**, 418 (2009).
[16] J. E. Han, O. Gunnarsson, and V. H. Crespi, Phys. Rev. Lett. **90**, 167006 (2003); M. Capone *et al.*, Phys. Rev. Lett. **93**, 047001 (2004).
[17] T. Takimoto *et al.*, J. Phys. Condens. Matter **14**, L369 (2002).
[18] The effect of Coulomb interaction on $\chi^c_{24,42}(\boldsymbol{q}, 0)$ is not large if $C_{ll',ll'} + C_{ll',l'l} = -U' + J + J'$ is small.
[19] λ_i for orbital $i = 2$–4 is $\lambda_i \approx -\sum_{j=2}^{4} N_j(0) V_{ij,ij}(0) = N(0)g(0)$, where $N_j(0)$ is the partial DOS. Then, $\lambda \approx N(0)g(0)$ in the band-diagonal basis.
[20] T. Shimojima *et al.*, Phys. Rev. Lett. **104**, 057002 (2010).
[21] F. Krüger *et al.*, Phys. Rev. B **79**, 054504 (2009); W. Lv, J. Wu, and P. Phillips, Phys. Rev. B **80**, 224506 (2009); C. C. Lee, W. G. Yin, and W. Ku, Phys. Rev. Lett. **103**, 267001 (2009).
[22] Above T_c, λ_E slightly increases with $n_{\rm imp}$ in conventional s-wave superconductors, but never exceeds unity.
[23] V. Mishra *et al.*, Phys. Rev. B **79**, 094512 (2009); D. Markowitz *et al.*, Phys. Rev. **131**, 563 (1963).
[24] D. V. Evtushinsky *et al.*, New J. Phys. **11**, 055069 (2009).
[25] T. Nakano *et al.*, Phys. Rev. B **81**, 100510(R) (2010); Y. Nakai *et al.*, Phys. Rev. B **81**, 020503(R) (2010).
[26] S. Kasahara *et al.*, arXiv:0905.4427.
[27] H. Kontani, Rep. Prog. Phys. **71**, 026501 (2008).
[28] Y. Yanagi *et al.*, Phys. Rev. B **81**, 054518 (2010).